JCTC Journal of Chemical Theory and Computation

Analysis of Bonding between Conjugated Organic Molecules and Noble Metal Surfaces Using Orbital Overlap Populations

Gerold M. Rangger,[†] Lorenz Romaner,[‡] Oliver T. Hofmann,[†] Georg Heimel,[§] Michael G. Ramsey,[||] and Egbert Zojer*,[†]

Institut für Festkörperphysik, Technische Universität Graz, Petersgasse 16, A-8010 Graz, Austria, Department Materialphysik, Montanuniversität Leoben, Franz-Josef-Strasse 18, A-8700 Leoben, Austria, Institut für Physik, Humboldt-Universität zu Berlin, Brook-Taylor-Strasse 6, D-12489 Berlin, Germany, and Institut für Physik, Karl Franzens Universität Graz, Universitätsplatz 5, A-8010 Graz, Austria

Received August 11, 2010

Abstract: The electronic structure of metal−organic interfaces is of paramount importance for the properties of organic electronic and single-molecule devices. Here, we use so-called orbital overlap populations derived from slab-type band-structure calculations to analyze the covalent contribution to the bonding between an adsorbate layer and a metal. Using two prototypical molecules, the strong acceptor 2,3,5,6-tetrafluoro-7,7,8,8-tetracyanoquinodimethane (F4TCNQ) on Ag(111) and the strong donor 1*H*,1′*H*-[4,4′]bipyridinylidene (HV0) on Au(111), we present overlap populations as particularly versatile tools for describing the metal−organic interaction. Going beyond traditional approaches, in which overlap populations are represented in an atomic orbital basis, we also explore the use of a molecular orbital basis to gain significant additional insight. On the basis of the derived quantities, it is possible to identify the parts of the molecules responsible for the bonding and to analyze which of the molecular orbitals and metal bands most strongly contribute to the interaction and where on the energy scale they interact in bonding or antibonding fashion.

1. Introduction

Over the past decade it has been increasingly acknowledged that the understanding of metal−organic interfaces is crucial for further improving organic (opto)electronic[1,2] and single-molecule devices.[3−5] In this context, adsorbing organic acceptors or donors onto electrodes provides a convenient tool for modifying metal work functions and consequently for tuning the alignment between the metal Fermi level and the organic semiconductor states.[6−14] A prototypical organic acceptor is 2,3,5,6-tetrafluoro-7,7,8,8-tetracyanoquinodimethane (F4TCNQ) (see right inset in Figure 1). F4TCNQ is a highly promising candidate for decreasing hole-injection barriers and has been thoroughly investigated in several spectroscopic and theoretical studies.[7−16] For efficiently decreasing electron-injection barriers, doubly reduced viologens have recently been suggested as particularly potent materials. This is especially true for 1*H*,1′*H*-[4,4′]bipyridinylidene, HV0 (see left inset in Figure 1), for which a very strong charge transfer to the Au(111) surface has been predicted theoretically.[17] This has later been confirmed experimentally for the more stable doubly methylated derivative 1,1′-dimethyl-[4,4′]bipyridinylidene. This material has been found to decrease the work function of a Au(111) surface by 2.2 eV[12] and to concomitantly decrease also the electron injection barrier into subsequently deposited organic electron transport layers such as C60 and Alq_3.[12]

* Corresponding author e-mail: egbert.zojer@tugraz.at.
[†] Technische Universität Graz.
[‡] Montanuniversität Leoben.
[§] Humboldt-Universität zu Berlin.
[||] Karl Franzens Universität Graz.

10.1021/ct100449c
Published on Web 09/30/2010

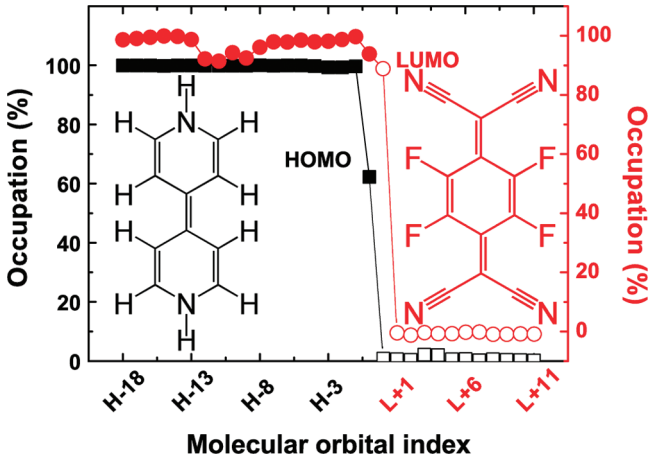

Figure 1. Comparison of the molecular orbital occupation of F4TCNQ on Ag(111) (circles), and HV0 on Au(111) (squares). The filled (open) symbols represent molecular orbitals that are occupied (unoccupied) in the isolated molecules. The right *y*-axis representing the occupations for F4TCNQ orbitals has been shifted by a constant to ease the comparison. The chemical structures of HV0 (left, 1*H*,1′*H*-[4,4′]bipyridinylidene) and F4TCNQ (right, 2,3,5,6-tetrafluoro-7,7,8,8-tetracyanoquinodimethane) are shown as insets. A more in-depth discussion of these data can be found in refs 16 and 17.

For both systems examined throughout this study, F4TCNQ on Ag(111) and HV0 on Au(111), the induced work-function modifications have been found to primarily originate from interfacial charge transfer. For F4TCNQ it is dominated by a nearly complete filling of the LUMO and for HV0 by a partial emptying of the HOMO.[12,16] A more in-depth understanding of the interfacial charge-transfer processes can be obtained from the density of states (DOS) projected onto the states of the monolayer without the metal present (i.e., essentially onto the orbitals of the noninteracting molecules). This quantity has been referred to as the "molecular orbital DOS".[18] Integrating the individual molecular orbital projected DOSs up to the Fermi level yields the occupation of the associated molecular states in the interacting system. The respective results for F4TCNQ on Ag(111) and HV0 on Au(111) are shown in Figure 1; an in-depth discussion of the molecular orbital DOSs of these systems can be found in refs 16 and 17. They indicate which molecular orbitals effectively gain or lose electrons upon adsorption. The underlying process that allows for fractional occupations is a hybridization of the molecular states with the metal states and the filling of only part of the resulting hybrid orbitals. The reduced occupation of the HOMO in HV0 on Au(111) and the nearly complete filling of the molecular LUMO for F4TCNQ on Ag(111) are clearly visible; for the latter, also a back-donation of electrons from deeper lying F4TCNQ orbitals to the Ag(111) surface is visible as a reduced occupation of the HOMO-12 to the HOMO-9. These states have been identified as being localized on the terminal CN substituents,[15,16] which is a first indication for the strong contribution of these groups to the metal−molecule bonding.

Their important role for the interaction can, furthermore, be deduced from the strong molecular distortions occurring upon adsorption that have been observed by X-ray standing wave experiments for F4TCNQ on Cu(111) and by density functional theory-based modeling on all coinage metals:[15,16] The F4TCNQ molecule, which is planar in gas phase, bends in a way that the terminal CN groups are closer to the surface by several tenths of an Angstrom than the central ring (with the absolute magnitude depending on the substrate metal). A bent adsorption geometry has recently been confirmed by scanning tunneling microscopy experiments on TCNQ (the nonfluorinated analogue to F4TCNQ) on Cu(100).[19] A nonvanishing (albeit much smaller) distortion has been calculated also for HV0 on Au(111).[17] In both cases, the bending gives rise to an intramolecular dipole which, in addition to the above-discussed charge transfer, determines the induced change in the substrate work function. The latter, amounting to +0.85 eV for F4TCNQ on Ag(111) and −1.21 eV HV0 on Au(111), is another indication for a strong metal−molecule interaction.[16,17]

Strong chemisorption usually leads to the establishment of (partial) bonds between the adsorbates and the substrate that goes hand in hand with a change of the bonding pattern within the adsorbed molecule. A technique to analyze these processes based on theoretical modeling was first introduced by Hoffmann et al.[18,20,21] They defined a crystal orbital overlap population (COOP) to interrogate the bonding and antibonding behavior of the atomic orbitals and their overlap with the metal bands resolved on the energy scale. In the present contribution, we describe what can be learned from such atomic orbital-based overlap populations about the covalent contributions to the bonding between organic adsorbates and metal surfaces by performing an in-depth analysis of the F4TCNQ/Ag(111) and HV0/Au(111) interfaces. Moreover, we expand the analysis tool to bonding and antibonding contributions arising from the interaction between certain molecular orbitals and the metal. These analyses allow identification of the individual atoms, the metal bands, and the molecular orbitals dominating the bonding process.

2. Methodology

All calculations presented here are based on optimized adsorption geometries obtained from the plane-wave density functional theory (DFT) code VASP, version 4.6.[22,23] Details on the applied methodology can be found in the respective papers dealing with the electronic structure of F4TCNQ and HV0 adorbates.[15−17] Here, the same unit cells as in those contributions are used, i.e.,

$$\begin{pmatrix} 4 & -1 \\ 4 & 0 \end{pmatrix}$$

for F4TCNQ on Ag(111) and $(3 \times 3^{1/2} \times 5)$ for HV0 on Au(111); the respective structures are included in the Supporting Information. To ease the projection onto atomic and molecular orbitals, we used the VASP geometries as an input to perform a single self-consistency cycle in the atomic orbital based code SIESTA[24] version 2.0. There, the PBE exchange−correlation functional, norm-conserving pseudopotentials based on relativistic calculations using the Troullier−Martins scheme, as well as the same $(3 \times 3 \times 1)$ Monkhorst−Pack[25] *k*-point grids (as

in the VASP calculations) were used. A double-ζ polarized (DZP) basis set with 15 atomic orbitals (AOs) for the metal atoms, 5 AOs for the hydrogen atoms, and 13 AOs for all other atoms has been used as implemented in the SIESTA code.[24,26,27] Test calculations applying a single-ζ polarized (SZP) basis as implemented in SIESTA[24] and a user-generated[28] triple-ζ polarized (TZP) basis with 21 AOs for the metal and 17 for the molecule (6 for H) were made to test the influence of the basis-set size on the obtained results. We found virtually identical results for the double- and triple-ζ basis sets. The single-ζ calculations yielded equivalent trends but resulted in some quantitative deviations, as discussed in the Supporting Information.

In this context it should be noted that, naturally, well-known shortcomings of density functional theory will to some extent adversely impact the full quantitative validity of the results in any such calculations. To minimize their role, we have, however, carefully chosen the test systems so that their impact should be comparably small. Moreover, they affect in no way the main purpose of the present paper, which is showing the versatility of orbital overlap populations for describing metal−molecule bonding. They can, of course, also be applied in future calculations that contain corrections to the flaws of current (semi)local DFT implementations.

The above-mentioned shortcomings include the neglect of van der Waals interactions by (semi)local functionals, which can lead to an overestimation of the bonding distance. During the past few years, several remedies to that problem have been discussed.[29] Here, to minimize its impact, we chose to study strongly bonded systems, where at least for F4TCNQ on Cu(111) a good agreement between theory and experiment has been observed.[15] Also the studied metal substrates were deliberately chosen among the coinage metals, as the charge transfer and interactions between a donor and Au (with the largest work function) and an acceptor and Ag (with the smallest work function) are particularly strong. Other effects including the lack of derivative discontinuity of the functionals,[30] the occurrence of self-interaction errors,[30] and improperly captured correlation-screening at the metal−organic interface[31,32] affect the relative alignment between the adsorbate and the metal states. In our test systems, this does at least not impact the positions of the frontier orbitals, for which it has been established theoretically and experimentally that they are pinned at the Fermi energy.[12,15−17] Also the positions and widths of the metal bands are known to be reasonably well described using relativistic pseudopotentials as in our calculations.[33−35]

3. Analysis of the Metal−Adsorbate Bonding

To elucidate the details of the bonding process, three different types of quantities are used: (i) densities of states (DOSs), (ii) orbital overlap populations (OoPs), and (iii) total overlap populations (ToPs).

(i) Densities of states in various forms are frequently applied to analyze interactions between adsorbate layers and metals. They give the numbers of states per energy interval either of the total system or projected onto a certain region of space (e.g., molecular density of states, metal density of states) or onto a volume element (local density of states). Alternatively, the projection can also be onto individual molecular orbitals of the noninteracting adsorbate (molecular-orbital-DOS), as discussed in Introduction (cf. Figure 1). A detailed DOS-based analysis of the HV0− and F4TCNQ− metal bonding can be found in refs 16 and 17.

(ii) Orbital overlap populations (OoPs) for analyzing bonds have originally been introduced by Hughbanks and Hoffmann[20] in the form of a crystal orbital overlap population (COOP). Its general definition is given by

$$\mathrm{OoP}_{\mathrm{X,Y}}(E) = \sum_{m\in \mathrm{X}, l\in \mathrm{Y}, i, \vec{k}} c^{*}_{im\vec{k}} c_{il\vec{k}} S_{ml\vec{k}} G(E - \varepsilon_{i\vec{k}}) \qquad (1)$$

Here, X and Y denote two groups of atoms and m and l the corresponding orbitals representing the basis set; the $c_{im\vec{k}}$ denote the linear combination of atomic orbital (LCAO) coefficients for state $\varepsilon_{i\vec{k}}$ and the $S_{ml\vec{k}}$ indicate the overlap matrices, where i is the band index. G is a line shape function, which in our case is a normalized Gaussian.

One can distinguish between different types of OoPs depending on which orbitals are included in the above summation; furthermore, one can sum over OoPs between different pairs of atoms or use different types of consistent basis sets, with respect to which the above expansion coefficients are defined. The latter results in different values for the S and c's in eq 1. The different types of OoPs used throughout this work are summarized in Table 1.

First, we will use atomic orbitals in line with the work by Hoffmann et al.,[18] which contains also a number of examples for the application of such OoPs to instructive test cases. Subsequently, we will combine the molecular orbitals of the isolated monolayer and the atomic orbitals of the metal slab to create a new basis[36] that is particularly useful for analyzing the interaction in a chemically intuitive way. A schematic illustration to explain this kind of OoP is provided in Figure 2, which shows how a molecular orbital interacts with a metal band. Among other effects, this causes a broadening of the orbital and the formation of hybrid states. Those that are of bonding character are typically located at energies below the original orbital, while antibonding states are located above. Hence, the OoP of the derived hybrid band is positive at low energies, cuts through zero at the position of the molecular orbital, and is negative at higher energies. This characteristic pattern is observed here for all molecular orbital-related OoPs (see section 4.3 and the corresponding Supporting Information), although the detailed shapes of the OoPs are usually more complex than in the schematic picture in Figure 2. Note that a very strong interaction with the substrate, such as the formation of covalent bonds, could result in deviations from this picture, if it causes a rehybridization of the states within the molecule. This is because in such a situation, the assumption of a single broadened molecular orbital is no longer appropriate.

(iii) To analyze the total contribution of the interaction between X and Y to the bonding in the investigated system, a total overlap population (ToP) can be introduced. It is defined as the integral over the corresponding OoP up to the Fermi energy; i.e., it is the integral over the "occupied" part of the respective OoP (cf., Figure 2). This quantity has been shown to scale with the bond order[18] and, consequently, is closely related to the bond length and the bonding strength.

Table 1. Definition of Orbital Overlap Populations Used throughout This Manuscript

intramolecular OoP	used in Supporting Information
Here, X and Y in eq 1 denote selected pairs of atoms within the molecule; *m* and *l* contain all AOs of the selected atoms. The resulting OoP then serves to analyze the bond between X and Y.	
metal−molecule OoP	used primarily in section 4.1
In this case, X refers to all atoms of the top two metal layers (the lower-lying layers do not contribute to the OoP) and Y to all atoms of the adsorbed molecule(s); *m* and *l* again include all related AOs. This quantity describes the overall bonding between the adsorbate layer and the metal substrate.	
metal$_{\text{"z"-band}}$−molecule OoP	used primarily in section 4.2
This quantity is equivalent to the metal−molecule OoP, with the exception that only specific orbitals are included in the summation over the metal atoms. In the present case, "z" = "s" and "z" = "d" will be studied to analyze the contributions from the metal s- and d-bands. Equivalently, one could also define an OoP in which only s- or p-type orbitals on the molecule are included; such an analysis would, however, be inferior to the metal−"molecular orbital" OoP discussed below.	
metal−molecule$_{\text{"part"}}$ OoP	used primarily in section 4.1
Here, the summation over Y runs only over a few selected atoms of the molecule(s). These can, for example, be the CN groups of F4TCNQ ("part " = "CN"). *m* and *l* again include all metal AOs and the AOs localized on the chosen part of the molecule, respectively. This quantity allows the study of bonding and antibonding interactions between a specific part of the molecule and the metal.	
metal− "molecular orbital" OoP	used primarily in section 4.3
This OoP allows partitioning of the metal−molecule OoP into contributions from specific molecular orbitals. It is defined such that X and *m* include all metal AOs and the $c_{im\vec{k}}$ are the corresponding LCAO coefficients. Y defines a single or a range of molecular orbitals, and the $c_{i\vec{l}\vec{k}}$ correspond to the linear combination of molecular orbital coefficients (LCMO).[36] This quantity allows identification of the contributions of chosen molecular orbital(s) to the metal−molecule OoP. For example, for "molecular orbital" = "HOMO", the bonding and antibonding overlap population between the molecular HOMO and the metal is obtained as a function of energy. In this context, it should be mentioned that summing over all the metal−"molecular orbital" OoPs recovers the metal−molecule OoP.	

ToPs can be calculated for all of the above-described OoPs and will be shown in the following whenever they provide additional insight. They will simply be denoted by replacing OoP with ToP in the quantities described in Table 1.

To avoid confusion, we will refrain from an excessive use of acronyms; i.e., we will write the "full" names of the above quantities apart from the acronyms OoP and ToP.

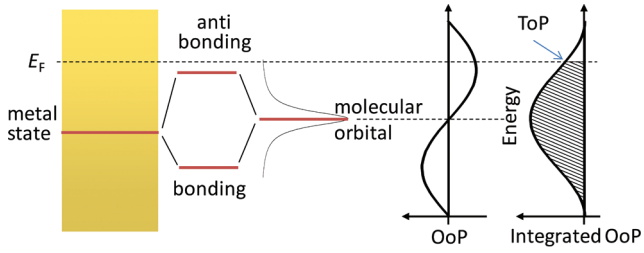

Figure 2. Schematic illustration of the interaction between a molecular orbital and a metal band giving rise to the metal−"molecular orbital" overlap population (OoP). The rightmost panel shows the OoP integrated over energy with the value of that curve at E_F corresponding to the total overlap population (ToP) associated with that orbital.

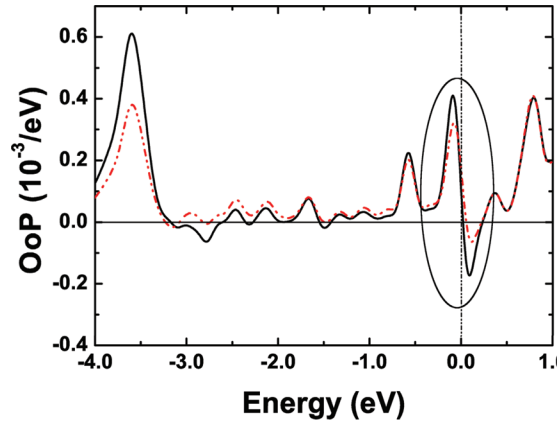

Figure 3. Metal−molecule OoP of HV0 on Au(111), black line. The dash-dot-dot line represents the metal−molecule$_{\text{part}}$ OoP where the part of the molecule consists of only the outer secondary amine groups with their hydrogen atoms. The Fermi edge is set to zero, and the horizontal line divides bonding (positive) and antibonding (negative) areas. The ellipse marks the area around E_F that is discussed in the main text.

4. Results and Discussion

The focus of the current manuscript is on using various types of overlap populations for analyzing the metal−molecule interactions. Therefore, in the main manuscript, we will refrain from discussing changes in the intramolecular OoP that occur due to adsorption-induced geometric deformations of the molecules.[15,17] The latter can, however, be found in the Supporting Information.

4.1. Orbital Overlap Population (OoP) between the Molecules and the Metal. *Bonding between HV0 and a Au(111) Surface.* As a first step, the metal−molecule OoP will be used to investigate the bonding between the molecules and the metal. The metal−molecule OoP of HV0 on Au(111) is shown as a black, solid line in Figure 3. Its shape around the Fermi energy is reminiscent of the "classical" situation described by Hoffmann for CO on Ni(100)[18] that is also sketched in Figure 2: The lower energy part of the band adopts a bonding and the upper energy part an antibonding character, as seen in the region marked by an ellipse in Figure 3. As the HOMO-derived band of the HV0 layer is only partially occupied due to the charge-transfer (cf., Introduction), it is not surprising that the Fermi energy depicted as a vertical dash-dotted line cuts right through the bonding to antibonding wave. At this point, only the significantly larger magnitude of the bonding feature might appear somewhat surprising. We will return to that and also identify the origin of the strongly bonding features at −0.6 eV and −3.6 eV, when discussing the molecular orbital−metal OoP for this system.

To identify the parts of the molecules that most strongly contribute to the metal−molecule interaction, metal−molecule "part" OoPs were calculated. The most relevant is the one associated with the two outer secondary amine groups together with their hydrogen atoms, the metal−molecule$_{\text{amine}}$ OoP. It is shown as a dash-dot-dotted line in Figure 3 and reproduces the positions of the main features of the metal−molecule OoP. This indicates that the secondary

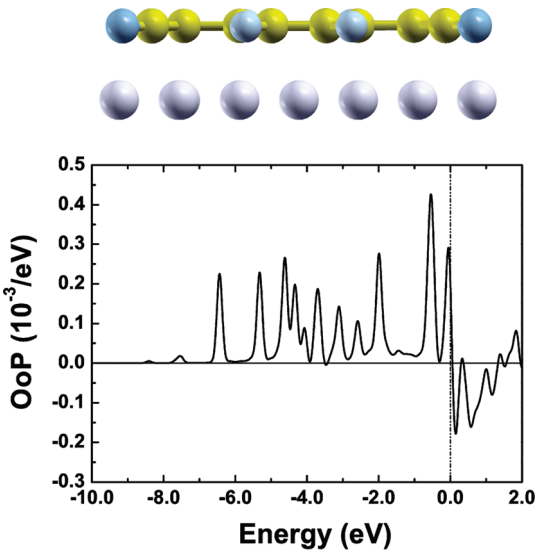

Figure 4. Metal−molecule OoP for the hypothetical case of a planar F4TCNQ monolayer adsorbed on Ag(111). The Fermi edge is set to zero, and the horizontal line divides bonding (positive) and antibonding (negative) areas. On top of the graph, a side view of an adsorbed planar F4TCNQ molecule is shown together with the top metal layer.

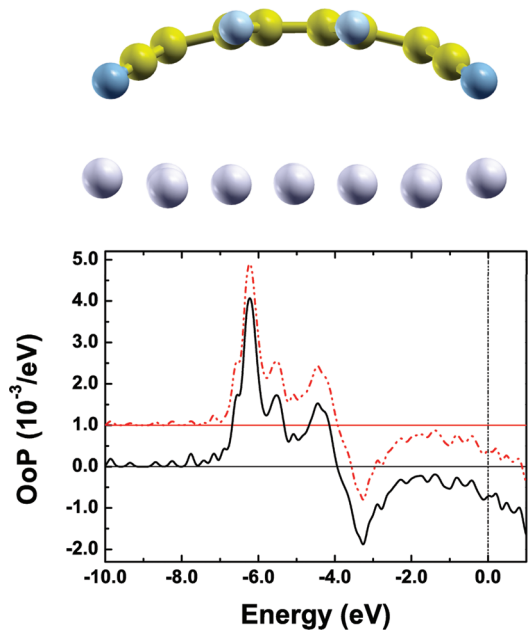

Figure 5. Metal−molecule OoP of F4TCNQ on Ag(111), black line, and metal−molecule$_{part}$ OoP of only the CN atoms of the molecule with the metal, red-shifted curve. The Fermi edge is set to zero and the horizontal line divides bonding (positive) and antibonding (negative) areas. On top of the plot, a side view of an adsorbed fully relaxed F4TCNQ molecule is shown together with the top metal layer.

amines are to a large extent responsible for the covalent contribution to the bonding between HV0 and Au. This can at least to some degree be associated with the calculated slight bending of the these groups toward the surface.[17]

OoP of F4TCNQ on Ag(111): The Impact of Bending. As the bending of the F4TCNQ molecules adsorbed on Ag(111) is much stronger,[16] it is advisable to first study the hypothetical case of a planar adsorbate (see structure in the top of Figure 4) and only as a second step investigate the impact of bending. The metal−molecule OoP for planar F4TCNQ on Ag(111) with the central ring at the same adsorption distance as in the fully relaxed structure (i.e., 3.21 Å above the metal)[16] is shown in Figure 4. A side view of the adsorbed molecule with the top metal layer is shown above the graph. The region around E_F looks qualitatively similar to HV0, with a bonding to antibonding transition. Also the absolute magnitude of the OoP peaks is comparable. Here, the features around E_F are related to the former LUMO which, due to the accepting nature of F4TCNQ, becomes slightly occupied. However, the amount of charge transfer is significantly lower than for the fully relaxed, bent adsorption geometry where a nearly complete filling of the LUMO has been observed as discussed in the introduction section and in ref 16.

The bending down of the terminal CN groups has dramatic consequences for the metal−molecule OoP. The result for the fully relaxed (i.e., strongly bent) adsorption geometry is shown in Figure 5 as a solid black line. Compared to the planar case in Figure 4, the whole region around E_F has become antibonding, and there is a strong negative peak at −3.3 eV. These are more than compensated by strongly bonding OoP contributions between −4.0 eV and −7.0 eV, which results in an increase of the corresponding total overlap population from 0.09 for the planarized adsorbate layer to 0.26 for the fully optimized case. It should be noted that the *y*-scales in Figures 3 and 4, on the one hand, and Figure 5, on the other hand, differ by a factor of 10(!).

Considering that the main difference between the planar and the fully optimized geometry is that in the latter the CN groups are bent down by 1.23 Å (position of the N-atoms), it is reasonable to assume that they must also be responsible for the huge changes in the OoP. This can be checked, by calculating the metal−molecule$_{CN}$ OoP in which only the interaction between the N and C atoms of the four terminal CN groups with the metal are considered. The corresponding OoP curve is shown as a dash, dot-dotted gray line in Figure 5. To be visible in the plot, the curve had to be shifted because the result is virtually identical to the full metal−molecule OoP. This confirms the leading contribution of the CN groups in the covalent part of the metal−molecule bonding in the fully relaxed geometry. This finding also implies that the prominent features in Figure 5 are related to molecular orbitals largely localized on the CN groups. A more in-depth analysis of the origin of the peaks addressing this question will be provided in section 4.3.

4.2. The Role of the Metal s- and d-Bands. In the next step, the role of the metal in the bonding process is investigated. The metal$_{s\ band}$−molecule and metal$_{d\ band}$−molecule OoPs for HV0 on Au(111) are shown in the top part of Figure 6. The corresponding ToPs are contained in the bottom part of Figure 6 for an extended energy range.

In this context it needs to be mentioned that in our calculations, the Au(111) d-band starts around −2 eV below E_F and has a width of 4.5 eV consistent with the calculations in ref 37. Interestingly, all strong d-band contributions to the overlap population have a positive sign below the Fermi edge. The metal$_{s\ band}$−molecule OoP starts contributing much

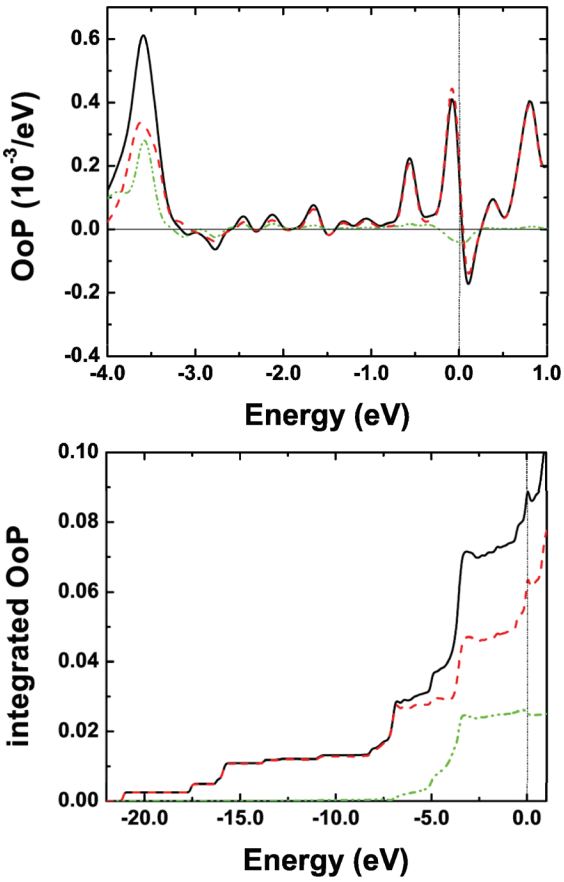

Figure 6. (top) Metal−molecule OoP (black, solid line) and $metal_{s,d\ band}$−molecule OoP of HV0 on Au(111) (top graph) and integrated metal−molecule and $metal_{s,d\ band}$−molecule OoP of HV0 on Au(111) (bottom graph). The red, dashed line represents the $metal_{s\text{-}band}$−molecule interaction, the green, dash, dot-dotted line the $metal_{d\text{-}band}$−molecule interaction. The vertical dash, dot-dotted line represents the Fermi energy, which is set to zero.

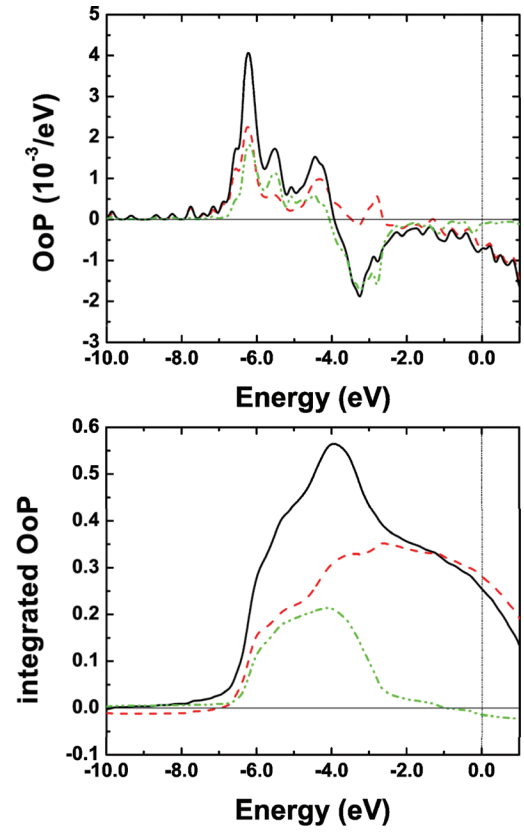

Figure 7. (top) Metal−molecule OoP (black, solid line) and $metal_{s,d\ band}$−molecule OoP of F4TCNQ on Ag(111) and (bottom) integrated metal−molecule (black, solid line) and $metal_{s,d\ band}$−molecule OoP of F4TCNQ on Ag(111). The red, dashed line represents the $metal_{s\text{-}band}$−molecule interaction, the green, dash, dot-dotted line the $metal_{d\text{-}band}$−molecule interaction. The vertical dash, dot-dotted line represents the Fermi energy, set to zero. The horizontal line in the top part divides bonding and antibonding contributions.

lower in energy (approximately −22 eV below E_F, which is attributed to the hybridization of low-lying molecular orbitals with parts of the metal s-band at higher energies). Its contributions to the overlap population are essentially bonding below the Fermi edge as well. As a result, about 2/3 of the metal−molecule ToP originates from the bonding to the Au s-electrons.

Qualitatively, a different pictures arises when studying the influence of the metal bands for the bonding process of F4TCNQ on Ag(111). In Ag, we calculate the onset of the d-band at ca. −3 eV (i.e., 1 eV lower than for Au) and the d-bandwidth as ca. 4 eV. Here, the interaction with the Ag d-band plays a strong role for the bonding OoP between −7 and −4 eV and even dominates the antibonding feature between −4 and −2 eV, as shown in Figure 7 (top), i.e., the interaction of the bent-down CN groups with the metal has a strong contribution from the Ag d-orbitals. The integral over the $metal_d$−molecule OoP in Figure 7 (bottom) reveals that the bonding and antibonding contributions largely cancel. In fact, in contrast to HV0 on Au(111) with its small positive $metal_d$−molecule ToP, here the antibonding d-band contributions slightly outweigh the bonding ones, resulting in a small negative $metal_d$−molecule ToP. This is far outweighed by the contribution from the s-band, for which especially the interaction with the CN groups is nearly exclusively bonding (Figure 7 (top)).

4.3. Molecular Orbital−Metal OoP. Finally, the molecular orbitals need to be identified, whose hybridization with the metal states gives rise to the various bonding and antibonding features in the above OoPs; i.e., we will discuss the metal− "molecular orbital" OoPs for HV0 on Au(111) and F4TCNQ on Ag(111). As in the present adsorbates, one frequently encounters groups of orbitals with similar character, we will "group" them in the following discussion for the sake of clarity. The corresponding OoPs for the individual orbitals can be found in the Supporting Information. The results for the OoPs associated with the most relevant (groups of) orbitals for HV0 on Au(111) are displayed in the left column of Figure 8. It is shown that the strongly bonding OoP of HV0 on Au(111) peaking at 3.6 eV is mostly a superposition of contributions from HOMO-3 and HOMO-2 derived states. Interestingly, an integration of the metal−HOMO-2 and metal−HOMO-3 OoPs shows that for these orbitals this strongly bonding peak is completely compensated by antibonding contributions closer to E_F (see right column of Figure 8). Also for the HOMO-1 (shown only in the Supporting Information), bonding and antibonding

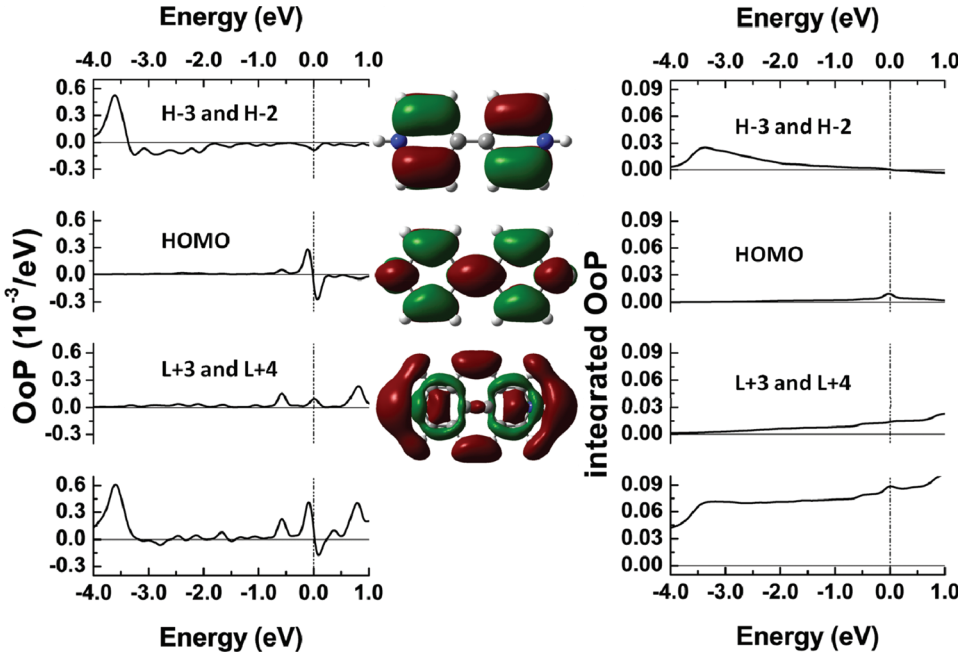

Figure 8. Left column: Metal−"molecular orbital" OoP analysis for HV0 on Au(111). The most significant (groups of) molecular orbitals and their OoPs with the metal are shown. From top to bottom: HOMO-2 plus HOMO-3, HOMO, LUMO+3 plus LUMO+4, and the total molecule−metal OoP; central column: shapes of the HOMO-2, the HOMO, and the LUMO+3 as representative examples; right column: corresponding integrated OoPs. ToPs and OoPs for all individual orbitals can be found in the Supporting Information.

features cancel and the ToP becomes zero. Of all occupied orbitals considered in Figure 8, only the metal−HOMO ToP does not vanish. The corresponding OoP, i.e., the metal−HOMO OoP is also responsible for the bonding to antibonding transition at E_F. However, it cannot explain its asymmetry as well as the magnitude of the peak at −0.6 eV. As shown in Figure 8, these features can only be rationalized by the partial occupation of unoccupied orbitals, namely the LUMO+3 and LUMO+4 (cf., Figure 1). Each of these orbitals displays a ToP contribution comparable to that of the HOMO. This is surprising, as the molecular orbital DOS of these two orbitals in Figure 1 shows that they do not bear significant electron density because they are filled to only about 2%[17] and, therefore, have received no attention in previous studies.[17] An orbital representation of these two states reveals the orbitals' σ-character and their large amplitudes around the secondary amine parts of the molecule. Exactly these parts of the molecule have been identified above to be of particular importance, when comparing the metal−molecule$_{amine}$ OoO to the metal−molecule OoP. Thus, as a net effect, the hybridization between metal states and unoccupied molecular states contributes more than 1/3 of the overall metal−molecule ToP, which is surprising for the adsorption of a strong electron donor. The rest of the ToP stems from deeper lying orbitals that are not included in Figure 8.

The analysis of the metal−"molecular orbital" OoP for F4TCNQ on Ag(111) confirms the notion that deep lying orbitals with large amplitudes on the CN groups are crucial for the development of the strong bond.[15,16] The metal−"molecular orbital" OoPs of the HOMO-12 to HOMO-9 (cf., Introduction) are responsible for the most strongly bonding feature at about −6.3 eV, as shown in the left column of Figure 9. However, they do not completely explain the bonding to antibonding transition at somewhat higher energies, which is mostly due to the contributions from the hybrid states formed by the HOMO-8 to HOMO-5 and the metal. Albeit the details of the shapes of the HOMO-12 to HOMO-9, the HOMO-8/HOMO-7, and the HOMO-6/HOMO-5 orbitals differ (see central column in Figure 9), they are all strongly localized on the terminal −CN group.

The LUMO-derived OoPs display a bonding to antibonding transition at −0.2 eV (similar to the HOMO-derived feature giving rise to a bonding to antibonding transition at about −1.2 eV; see Supporting Information). Compared to the OoPs related to HOMO-12 to HOMO-5, the respective contributions are, however, so weak that they are hardly visible in the metal−molecule OoP.

An analysis of the corresponding ToPs displayed in the right column of Figure 9 shows that, not unexpectedly, the dominant contribution to the covalent part of the metal−molecule bonding comes from the HOMO-12 to HOMO-9 contributions.

4.4. Comparison between Orbital Overlap Populations and the DOS Projected onto the Molecular Region. Finally, the relation between the metal−molecule OoP and the DOS projected onto the molecular region need to be discussed. Here, one has to keep in mind that the prerequisite for a nonvanishing metal−molecule OoP in a certain energy region is that there metal−molecule hybrid orbitals must exist, i.e., the region will typically be close to the respective bands of the isolated molecular layer and metal slab. Moreover, the orbitals on the molecule and the metal need to overlap, which finds its mathematical manifestation in the overlap integral in eq 1. Keeping that in mind, the similarities and differences between the molecular DOS and

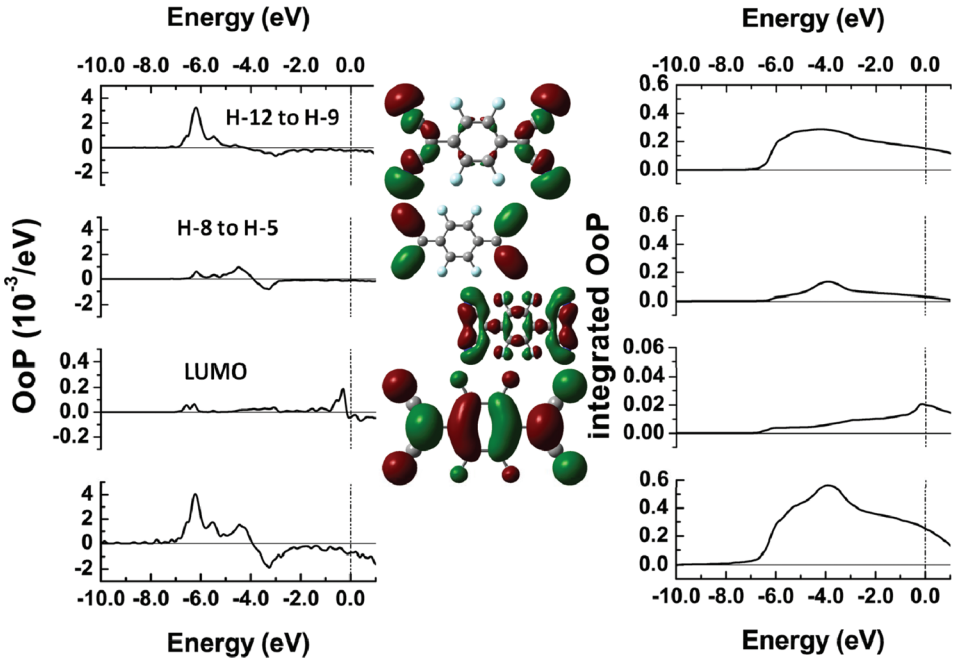

Figure 9. Left column: Metal−"molecular orbital" OoP analysis for F4TCNQ on Au(111). The most significant (groups of) molecular orbitals and their OoPs with the metal are shown. From top to bottom: Sum of HOMO-12 to HOMO-9, sum of HOMO-8 to HOMO-5, LUMO and the total molecule-metal OoP. Note that the scale for the metal−LUMO OoP differs from the others by a factor of 10. Central column: shapes of the HOMO-9, the HOMO-7, the HOMO-5, and the LUMO shown as representative examples; right column: corresponding integrated OoPs. ToPs and OoPs for all individual orbitals can be found in the Supporting Information.

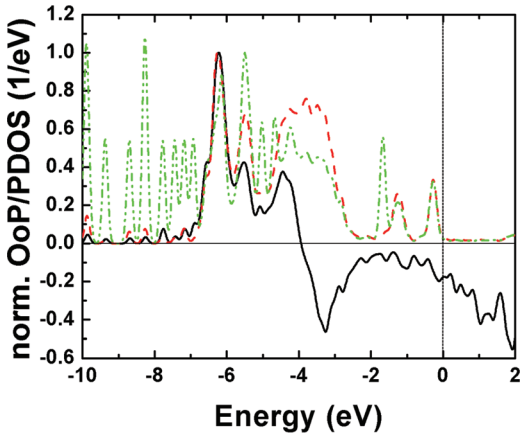

Figure 10. Normalized metal−molecule OoP (black solid line), DOS projected onto the molecular region (green dash-dotted line), and DOS projected onto the region around the N-atoms (red dashed line) for F4TCNQ adsorbed on Ag(111).

the metal−molecule OoP can be well understood and are shown in Figure 10 for the example of F4TCNQ on Ag(111).

The dominant metal−molecule OoP features between −7.0 and −2.5 eV correlate well with an energy range of increased DOS in the molecular region, especially in the region around the downward bent N-atoms (green dash-dotted and red-dashed line in Figure 10, respectively) and a very large DOS in the metal in exactly that energy range due to the d-bands (vide supra). Also for the features at higher energies, a correlation with the DOS projected on the N-atoms and the metal−molecule OoP is well visible. The overall magnitude of the OoP is, however, somewhat lower due to the lack of metal-d-band contributions. The bonding to antibonding transitions in the OoP are, of course, not visible in the DOS. Figure 10 also shows that the OoP is clearly different from a DOS simply separated into bonding to antibonding contributions. This is evidenced, for example, by only very small OoP peaks associated with the DOS maxima below −6.8 eV and at −1.8 eV that are not associated with the downward-bent N-atoms, which manifests itself in small overlap integrals and, thus, in a reduced OoP.

5. Conclusions

We introduce a number of versatile tools for analyzing the covalent contribution to the bonding between organic adsorbates and metal surfaces that are derived from the crystal orbital overlap population introduced by Hoffmann et al.[18] These tools allow the identification of energies at which metal−molecule hybrid states have bonding and antibonding character, respectively, and together with the calculation of a total overlap population they provide a measure for the total covalent bonding strength. Overlap populations enable the identification of the atoms and groups of the molecule that most strongly contribute to the bonding and also make it possible to quantify the role of different metal bands as well as (sets of) molecular orbitals in the bonding process.

As instructive examples, we apply various overlap populations to explain the bonding between a particularly strong electron donor, HV0, and Au(111) and the prototypical acceptor F4TCNQ and Ag(111). For the former example, they highlight the contribution of otherwise easily overlooked unoccupied orbitals that become only slightly occupied in the course of the bonding but have large amplitudes on those

parts of the molecules that are closest to the metal. For F4TCNQ on Ag(111), the pivotal contribution of the terminal CN groups and the orbitals localized on those groups is identified.

Acknowledgment. The authors acknowledge the financial support by the Austrian Fonds zur Förderung der Wissenschaftlichen Forschung (FWF) project P20972-N20 and the European Commission project "IControl" (EC-STREP-033197). The authors thank H. Sormann for performing test-calculations of metal band structures.

Supporting Information Available: Figure showing the structure of the unit-cell for F4TCNQ on Ag(111) and HV0 on Au(111). Comparison of the metal−molecule OoP for these systems calculated with single-, double-, and triple-ζ basis sets. Discussion of changes in the intramolecular OOP; metal−"molecular orbital" OoPs for individual molecular orbitals and corresponding shapes of orbitals. This material is available free of charge via the Internet at http://pubs.acs.org.

References

(1) Ishii, H.; Sugiyama, K.; Ito, E.; Seki, K. *Adv. Mater.* **1999**, *11*, 605.

(2) Koch, N. *ChemPhysChem* **2007**, *8*, 1438.

(3) Patrone, L.; Palacin, S.; Charlier, J.; Armand, F.; Bourgoin, J. P.; Tang, H.; Gauthier, S. *Phys. Rev. Lett.* **2003**, *91*, 096802.

(4) Yaliraki, S. N.; Kemp, M.; Ratner, M. A. *J. Am. Chem. Soc.* **1999**, *121*, 3428.

(5) Seminario, J. M.; De La Cruz, C. E.; Derosa, P. A. *J. Am. Chem. Soc.* **2001**, *123*, 5616.

(6) Werner, A. G.; Li, F.; Harada, K.; Pfeiffer, M.; Fritz, T.; Leo, K. *Appl. Phys. Lett.* **2003**, *82*, 4495.

(7) Koch, N.; Duhm, S.; Rabe, J. P.; Vollmer, A.; Johnson, R. L. *Phys. Rev. Lett.* **2005**, *95*, 237601.

(8) Chan, C. K.; Kim, E. G.; Brédas, J. L.; Kahn, A. *Adv. Funct. Mater.* **2006**, *16*, 831.

(9) Duhm, S.; Glowatzki, H.; Cimpeanu, V.; Klankermayer, J.; Rabe, J. P.; Johnson, R. L.; Koch, N. *J. Phys. Chem B* **2006**, *110*, 21069.

(10) Jackel, F.; Perera, U. G. E.; Iancu, V.; Braun, K. F.; Koch, N.; Rabe, J. P.; Hla, S. W. *Phys. Rev. Lett.* **2008**, *100*, 126102.

(11) Lindell, L.; Unge, M.; Osikowicz, W.; Stafstrom, S.; Salaneck, W. R.; Crispin, X.; de Jong, M. P. *Appl. Phys. Lett.* **2008**, *92*, 163302.

(12) Bröker, B.; Blum, R. P.; Frisch, J.; Vollmer, A.; Hofmann, O. T.; Rieger, R.; Mullen, K.; Rabe, J. P.; Zojer, E.; Koch, N. *Appl. Phys. Lett.* **2008**, *93*, 243303.

(13) Bröker, B.; Blum, R.-P.; Beverina, L.; Hofmann, O. T.; Sassi, M.; Ruffo, R.; Pagani, G. A.; Heimel, G.; Vollmer, A.; Frisch, J.; Rabe, J. P.; Zojer, E.; Koch, N. *ChemPhysChem* **2009**, *10*, 2947.

(14) Mukai, K.; Yoshinobu, J. *J. Electron Spectrosc.* **2009**, *174*, 55.

(15) Romaner, L.; Heimel, G.; Bredas, J.-L.; Gerlach, A.; Schreiber, F.; Johnson, R. L.; Zegenhagen, J.; Duhm, S.; Koch, N.; Zojer, E. *Phys. Rev. Lett.* **2007**, *99*, 256801.

(16) Rangger, G. M.; Hofmann, O. T.; Romaner, L.; Heimel, G.; Bröker, B.; Blum, R.-P.; Johnson, R. L.; Koch, N.; Zojer, E. *Phys. Rev. B* **2009**, *79*, 12.

(17) Hofmann, O. T.; Rangger, G. M.; Zojer, E. *J. Phys. Chem. C* **2008**, *112*, 20357.

(18) Hoffmann, R. *Rev. Mod. Phys.* **1988**, *60*, 601.

(19) Santato, C.; Rosei, F. *Nat. Chem.* **2010**, *2*, 344.

(20) Hughbanks, T.; Hoffmann, R. *J. Am. Chem. Soc.* **1983**, *105*, 1150.

(21) Wijeyesekera, S. D.; Hoffmann, R. *Organometallics* **1984**, *3*, 949.

(22) Kresse, G.; Furthmuller, J. *Comput. Mater. Sci.* **1996**, *6*, 15.

(23) Kresse, G.; Furthmüller, J. *Phys. Rev. B* **1996**, *54*, 11169.

(24) Soler, J. M.; Artacho, E.; Gale, J. D.; Garcia, A.; Junquera, J.; Ordejon, P.; Sanchez-Portal, D. *J. Phys.: Condens. Matter* **2002**, *14*, 2745.

(25) Monkhorst, H. J.; Pack, J. D. *Phys. Rev. B* **1976**, *13*, 5188.

(26) Junquera, J.; Paz, Ó.; Sánchez-Portal, D.; Artacho, E. *Phys. Rev. B* **2001**, *64*, 235111.

(27) García-Gil, S.; García, A.; Lorente, N.; Ordejón, P. *Phys. Rev. B* **2009**, 79–075441.

(28) Artacho, E.; Gale, J. D.; Garcia, A.; Junquera, J.; Martin, R. L.; Ordejon, P.; Sanchez-Portal, D.; Soler, J. M. User's Guide SIESTA 2.0; 2006, p 82.

(29) Tkatchenko, A.; Romaner, L.; Hofmann, O. T.; Zojer, E.; Ambrosch-Draxl, C.; Scheffler, M. *MRS Bull.* **2010**, *35*, 435.

(30) Kümmel, S.; Kronik, L. *Rev. Mod. Phys.* **2008**, *80*, 3.

(31) Newns, D. M. *Phys. Rev.* **1969**, *178*, 1123.

(32) Neaton, J.; Hybertsen, M.; Louie, S. *Phys. Rev. Lett.* **2006**, *97*, 216405. Li, Y.; Lu, D.; Galli, G. *J. Chem. Theory Comput.* **2009**, *5*, 881.

(33) Marini, A.; Onida, G.; Del Sole, R. *Phys. Rev. Lett.* **2001**, *88*, 016403.

(34) Marini, A.; Onida, G.; Del Sole, R. *Phys. Rev. B* **2001**, *64*, 195125.

(35) Speer, N. J.; Brinkley, M. K.; Liu, Y.; Wei, C. M.; Miller, T.; Chiang, T.-C. *Europhys. Lett.* **2009**, *88*, 67004.

(36) Rangger, G. M.; Romaner, L.; Heimel, G. *Zojer Surf. Interface Anal.* **2008**, *40*, 371.

(37) Di Felice, R.; Selloni, A.; Molinari, E. *J. Phys. Chem. B* **2002**, *107*, 1151.

CT100449C